Weather and Climate Extremes 11 (2016) 28–40

Contents lists available at ScienceDirect

Weather and Climate Extremes

journal homepage: www.elsevier.com/locate/wace

Projecting changes in regional temperature and precipitation extremes in the United States

Justin T. Schoof [a,*], Scott M. Robeson [b]

[a] Department of Geography and Environmental Resources, Southern Illinois University, Carbondale, IL 62901, USA
[b] Department of Geography, Indiana University, Bloomington, IN 47405, USA

ARTICLE INFO

Article history:
Received 26 June 2015
Received in revised form
22 September 2015
Accepted 28 September 2015
Available online 9 October 2015

Keywords:
Extremes
Regional climate
Downscaling
Quantile mapping

ABSTRACT

Regional and local climate extremes, and their impacts, result from the multifaceted interplay between large-scale climate forcing, local environmental factors (physiography), and societal vulnerability. In this paper, we review historical and projected changes in temperature and precipitation extremes in the United States, with a focus on strengths and weaknesses of (1) commonly used definitions for extremes such as thresholds and percentiles, (2) statistical approaches to quantifying changes in extremes, such as extreme value theory, and (3) methods for post-processing (downscaling) global climate models (GCMs) to investigate regional and local climate. We additionally derive regional and local estimates of changes in temperature extremes by applying a quantile mapping approach to high-resolution gridded daily temperature data for 6 U.S. sub-regions. Consistent with the background warming in the parent GCMs, we project decreases in regional and local cold extremes and increases in regional and local warm extremes throughout the domain, but the downscaling approach removes bias and produces substantial spatial variability within the relatively small sub-regions. We finish with recommendations for future research on regional climate extremes, suggesting that focus be placed on improving understanding of extremes in the context of large-scale circulation and evaluating the corresponding cascade of scale interactions within GCMs.

1. Introduction

Regional weather and climate extremes – unusual values of one or more variables for a specific geographic region and time of year – have substantial societal and economic impacts each year. Temperature extremes are closely linked to impacts on human health (Patz et al., 2005; O'Neill and Ebi, 2009; Mishra et al., 2015), short-term energy supply and demand (Schaeffer et al., 2012), transportation (Rowan et al., 2013), and many other sectors (Sivakumar, 2013). Precipitation extremes have widespread implications for agriculture (Anyamba et al., 2014) and transportation as well as flooding and urban drainage systems (Rosenberg et al., 2010). This paper aims to provide an overview of current issues associated with developing regional climate projections using global climate model (GCM) scenarios, with a focus on temperature and precipitation extremes in the United States.

Analyses that focus on changes in extremes within the observational record have identified widespread changes in the tails of the temperature distribution that are consistent with large-scale warming (Donat et al., 2013). Generally, changes in extremes associated with minimum temperature have been larger than those for maximum temperature, although recent warming (last 30 years) has been characterized by larger increases in warm anomalies relative to cold anomalies (Robeson et al., 2014). There have also been increases in precipitation extremes in many regions, but with less spatial homogeneity than temperature changes (Donat et al., 2013). Many land areas, including most regions within the United States, are characterized by positive trends in precipitation frequency and/or intensity (Alexander et al., 2006; Griffiths and Bradley, 2007; Groisman and Knight, 2007; Groisman et al., 2012; Donat et al. 2013; Guilbert et al., 2015). A growing body of evidence attributes large-scale changes in the frequency and/or intensity of temperature and precipitation extremes to radiative forcing from greenhouse gases (Christidis et al., 2011; Min et al., 2011; Zwiers et al., 2011) and highlights the need to quantify potential societal impacts from future changes.

In order to mitigate the impacts of changes in extremes, we must understand how such changes are manifested at the local to regional scale. This requires methods and approaches that are distinct from those used for the detection and attribution of extreme events. Model bias and the specific spatial scale of interest are critical considerations in this process. As an example, the

* Corresponding author.
E-mail address: jschoof@siu.edu (J.T. Schoof).

http://dx.doi.org/10.1016/j.wace.2015.09.004

comparison of point precipitation observations to output from GCMs has promoted the notion of the "drizzle problem", whereby models show an altered probability distribution that has higher precipitation frequency and lower precipitation intensity. While not always interpreted in this way, the high frequency of precipitation in GCMs relative to station observations is not a model shortcoming, but instead the result of the difference in spatial scale (and also occurs in gridded observational precipitation; Ensor and Robeson, 2008). Contemporary GCMs, such as those used for the 5th Coupled Model Intercomparison Project (CMIP5; Taylor et al., 2012) are a key component of regional climate change projections, but their limited spatial resolution reduces their utility in estimating local or regional extremes without substantial post-processing (this is especially true in regions of large relief). Such post-processing typically includes bias correction as well as statistical or dynamical modeling, which is often referred to as downscaling.

The objective of this paper is to review the approaches used to project future climate extremes at the regional-to-local scale. While projections can be developed for a range of climatic variables, we focus on temperature and precipitation events at the daily timescale because of their climatic importance and clear societal impacts. The rest of the paper is organized as follows. Section 2 reviews existing metrics used to define temperature and precipitation extremes. Section 3 summarizes methods for developing high resolution projections of extremes given coarse output from contemporary GCMs. Section 4 describes results from previous studies engaged in projection of regional climate extremes for the US. In Section 5, examples of newly developed high resolution projections of regional temperature extremes are presented. The final section includes recommendations for future work.

2. Defining extremes

Given a climatic time series, extremes can be defined in many different ways. The simplest and most common approaches are based on threshold exceedances, such as the number of days for which the minimum temperature is below freezing. At a given location, approaches based on thresholds are easy to understand, but they make assessment of spatial patterns of changes in extremes difficult as they are not equally applicable in all climates (Wehner et al., 2013a) and can change relatively quickly with elevation or proximity to large water bodies. Percentile-based approaches, where the percentiles are defined in a spatially varying manner, such as the number of days exceeding the 95th percentile at a given location, are more amenable to exploring spatial variations in extremes. Several variations on threshold and percentile-based metrics were developed under the auspices of the World Meteorological Organization Commission for Climatology (CCl)/World Climate Research Programme (WCRP) project on Climate Variability and Predictability (CLIVAR) Expert Team on Climate Change Detection and Indices (ETCCDI) as described by Frich et al. (2002), Alexander et al. (2006) and Zhang et al. (2011). These are commonly referred to as the ETCCDI indicators and are summarized in Table 1.

The advantages of the ETCCDI indicators are that they are easy to interpret and are directly related to impacts in agriculture and other sectors. Furthermore, gridded ($2.5^\circ \times 3.75^\circ$) monthly and annual time series of the indicators have been made available as HadEX (Alexander et al., 2006) and HadEX2 (Donat et al., 2013). This makes them ideal for analysis of trends in extremes over large regions (e.g., Hartmann et al., 2013) and for comparison to extremes in output from GCMs (e.g., Collins et al., 2013). While some of the ETCCDI indicators are not indicative of truly extreme events (e.g., minimum temperatures below freezing are not extreme in most high latitude regions; Wehner et al., 2013a; Sato and Robeson, 2014), changes in their values represent changes in conditions that are likely to be accompanied by societal impacts. While the ETCCDI indicators include a few metrics aimed at changes in precipitation persistence, they are not well suited for characterizing changes in drought. They can therefore be supplemented by widely used drought indices, such as the Palmer Drought Severity

Table 1
List of indicators devised by the ETCCDI (see Section 2). T_{max} and T_{min} refer to daily maximum and minimum temperature, respectively. Shaded indicators are used in Section 5.

Indicator name	Abbrev.	Definition
Frost days	FD	Number of days with $T_{min} < 0$ °C
Icing days	ID	Number of days with $T_{max} < 0$ °C
Summer days	SU	Number of days with $T_{max} > 25$ °C
Tropical nights	TR	Number of days with $T_{min} > 20$ °C
Cool nights	TN10p	% of days with $T_{min} <$ the historical 10th percentile value
Warm nights	TN90p	% of days with $T_{min} >$ the historical 90th percentile value
Cool days	TX10p	% of days with $T_{max} <$ the historical 10th percentile value
Warm days	TX90p	% of days with $T_{max} >$ the historical 90th percentile value
Maximum T_{min}	TNx	Monthly maximum value of T_{min}
Minimum T_{min}	TNn	Monthly minimum value of T_{min}
Maximum T_{max}	TXx	Monthly maximum value of T_{max}
Minimum T_{max}	TXn	Monthly minimum value of T_{max}
Diurnal range	DTR	Monthly mean difference between daily T_{max} and T_{min}
Growing season length	GSL	Number of days between the first 6-day span with daily mean temperature above 5 °C and the first span after July 1 (in NH) with daily mean temperature below 5 °C
Warm spell duration index	WSDI	Annual count of at least six consecutive days with $T_{max} >$ the historical 90th percentile value
Cold spell duration index	CSDI	Annual count of at least six consecutive days with $T_{min} <$ the historical 10th percentile value
Maximum 1-day precipitation	RX1day	Monthly maximum 1-day precipitation (mm)
Maximum 5-day precipitation	RX5day	Monthly maximum consecutive 5-day precipitation amount (mm)
Simple daily intensity index	SDII	Mean precipitation amount on wet days (mm)
Number of heavy precipitation events	R10	Annual count of days with precipitation >10 mm
Number of very have precipitation days	R20	Annual count of days with precipitation >20 mm
Consecutive dry days	CDD	Maximum number of consecutive days with precipitation <1 mm
Consecutive wet days	CWD	Maximum number of consecutive days with precipitation >1 mm
Very wet days	R95p	Annual total precipitation derived from days >95th percentile
Extremely wet days	R99p	Annual total precipitation derived from days >99th percentile
Annual total precipitation	PRCPTOT	Annual total precipitation on all days.

Index (PDSI) or Crop Moisture Index (CMI), or even changes in seasonal temperature averages or precipitation totals, to translate projections of extremes into terms that might be better understood by stakeholders.

An alternative to the ETCCDI indicators is the use of return periods, or alternatively, return values. As an example, to estimate an annual return value for extreme daily precipitation, the τ-year return value is defined as the daily precipitation total with a $1/\tau$ probability of occurring in any given year (Kharin et al., 2007). Return-period and return-value approaches are better suited for investigating changes in events that are more unusual than most of the ETCCDI indicators (Brown et al., 2008; Wehner et al., 2013a). Such approaches usually are based in extreme-value theory as described in Section 3.

3. Review of methods for projecting changes in regional climate extremes

3.1. Regional climate change projections

The scale dependence of extremes coupled with the coarse resolution of contemporary GCMs limits the applicability of using raw GCM output to analyze changes in extremes at scales smaller than subcontinental regions (and even at large spatial scales, GCMs have biases that should be removed). As a result, analysis of changes in regional and local extremes requires downscaled GCM output. The goal of downscaling is to derive high resolution climate information that is consistent with simulations from coarse resolution GCMs. Downscaling methods usually are defined as either dynamical (i.e., regional climate modeling) or statistical, although the increasingly widespread availability of regional climate model output has resulted in an increasing number of studies that apply statistical post-processing to high resolution output from dynamical models (e.g., Gudmundsson et al., 2012). Several studies have also combined statistical and dynamical downscaling by performing weather typing and then applying RCMs to explore regional climate associated with specific circulation regimes (e.g., Reyers et al., 2013).

Dynamical downscaling is conducted by using lateral boundary conditions from a GCM with a high-resolution dynamical model over a regional domain or by conducting high resolution time-slice experiments for the globe. The advantages of dynamical downscaling are the physical consistency of individual variables and internal consistency among variables. The primary disadvantages of dynamical downscaling are computational time and potential model bias. Practitioners must also be cognizant of any limitations associated with the data used to provide lateral boundary conditions, as well as any parameterizations (Mannig et al., 2013) that may not be applicable in other climatic regimes.

Statistical downscaling most commonly develops historical relationships between station data (or high resolution gridded products) and large-scale circulation variables and then applies these relationships to output from transient GCM simulations (see Maraun et al. (2010) and Schoof (2013) for reviews of statistical downscaling). Methods for statistical downscaling range from simple regression approaches to artificial neural networks and machine-learning algorithms. Most statistical downscaling approaches include a bias-correction step, either implicitly (as is common in regression-based approaches, which account for differences in central tendency) or explicitly in quantile-mapping approaches (such as bias correction and spatial disaggregation, BCSD; Wood et al., 2004). The primary advantage of statistical downscaling is ease of application, which allows methods to be applied to multiple GCMs and multiple greenhouse gas emissions pathways to investigate the uncertainty space associated with regional climates (see Hawkins and Sutton (2009)). For statistical downscaling, the quality of the observational data is primary consideration, as is the stationarity of the relationship between regional/local scale climate and large-scale circulation.

Temperature and precipitation biases in GCM simulations can be large and are often inherited by regional models in the process of dynamical downscaling. Before GCM or RCM output can be used to assess climate change impacts, bias correction is necessary. As noted above, regression-based downscaling methods implicitly correct for bias in the mean but not necessarily for other parts of the frequency distribution. Quantile mapping (Panofsky and Brier, 1968) has emerged as a common approach for correcting GCM biases across the empirical cumulative distribution function (ecdf). In this approach, quantile-specific biases are determined by comparing observations with either GCM or RCM output under historical forcings. Under the assumption that the bias is time-invariant, the same quantile-specific bias correction is applied to GCM or RCM output using different forcings, such as those associated with elevated concentrations of greenhouse gases. When quantile mapping is done between coarse resolution GCM data and higher resolution station data or gridded fields, it also serves as a statistical downscaling method (Abatzoglou and Brown, 2012).

In a downscaling context, quantile mapping can be problematic for some phenomena that have high spatial variability at the sub-GCM-grid scale, such as precipitation. As demonstrated by Maraun (2013), a rain event within a GCM or RCM grid box is not likely to impact all locations within the grid box in the same way, but a quantile mapping approach will necessarily translate a given GCM or RCM value to the same quantile along the ecdf of all locations within the grid box. Maraun (2013) proposes the use of a stochastic bias correction to overcome this problem. Thrasher et al. (2012) noted that quantile mapping of maximum and minimum temperatures can lead to unrealistic values of diurnal temperature range (DTR), suggesting that DTR and then either maximum or minimum temperature should be used in the bias correction. There also is the question of how to handle quantiles in GCM simulations that are smaller or larger than those that occur in the historical data. With careful attention to these issues, however, quantile mapping is among the most useful bias-correction approaches in the climate-science toolbox (Gudmundsson et al., 2012; Teutschbein and Seibert, 2012).

3.2. Approaches for quantifying extremes

Several options exist for quantifying future regional climate extremes associated with high-resolution, bias-corrected GCM or RCM output. The most common methods for deriving projections of future extremes are associated with either empirical (i.e., based on changes in indicators such as those in Table 1) or functional (i.e., based on fitting functions to the tails of the probability distribution) approaches. The first approach is straightforward: given historical and future climate data, the indicators can be tallied and maps of differences presented. Application of extreme value theory (EVT) is more complex, so a brief overview is provided here. Readers are directed to Coles (2001) for a more complete treatment.

The two most common approaches to EVT are the block-maxima approach and the peaks-over-threshold approach. In the former, a block of time (e.g., a year) is chosen and the set of maxima from all blocks forms the sample. Using one of the three forms of the generalized extreme-value distribution (Gumbel, Fréchet, or Weibull), a function is fit to the extreme values that form the sample (e.g., Kharin et al., 2007). In the peaks-over-threshold approach, a threshold is specified and all events meeting the criteria form the sample that is analyzed using a generalized Pareto distribution. The latter approach is particularly useful if multiple

extremes occur within one block (Brown et al., 2008), but care must be taken to avoid biased samples (i.e., including multiple events that are derived from the same forcing event). Since parameters of these distributions have little meaning among non-statisticians, results of extreme-value approaches are most often presented in terms of return periods or values (Wehner, 2013a), although EVT approaches have also been applied to some of the ETCCDI indicators (e.g., Peterson et al., 2013). In general, EVT methods perform well with heavy-tailed distributions, where typical interpretations of standard-deviation units or even percentiles may not be appropriate. Since the notion of a return period is based on an assumption of stationarity, additional steps are required to apply EVT in the context of climate change. Several approaches that include time dependence have been described in the climate science literature (Kharin and Zwiers 2005; Wehner, 2013a; Cheng et al., 2014) and elsewhere (Huerta and Sansó 2007).

4. Review of findings from previous regional studies

Theoretical and observational studies have linked large-scale changes in extreme temperature and precipitation to changes in background warming (e.g., Sillmann et al., 2013a, 2013b). In the case of temperature, an increase in the mean leads to an increase in warm extremes, in the absence of a strong negative variance response (Robeson, 2002). Increases in atmospheric moisture content associated with warming are producing changes in the frequency and intensity of precipitation with the theoretical expectation that extremes will change more than the mean (see discussion in Trenberth et al. (2003), Emori and Brown (2005) and O'Gorman and Schneider (2009)). However, natural variability (Grotjahn et al., 2015) and regional processes also play an important role in determining changes in extremes. For example, temperature extremes are closely linked to local hydrologic processes and region-specific teleconnections (Diffenbaugh et al., 2005; Ford and Quiring, 2014). Precipitation extremes are similarly sensitive to surface-atmosphere interaction as well as changes in atmospheric circulation that result in changes in regional moisture advection and convergence.

Historical analyses and projections of climate extremes have been developed for many U.S. regions, often using the output from coordinated modeling experiments such as CMIP5 with the ETCCDI indicators or other measures (e.g., Sillmann et al., 2013b and Wuebbles et al., 2013 for global and U.S. perspectives, respectively). Because regional studies tend to use different metrics, GCMs, and time periods, direct comparisons are difficult. The focus here is therefore on the relatively few studies that have evaluated regions using consistent definitions, data, and time periods for analysis (e.g., Donat et al., 2013; Kunkel et al., 2013b). Of particular interest for the projection of extremes are results from the North American Regional Climate Change Assessment Program (NARCCAP; Mearns et al., 2009). NARCCAP employed multiple GCM-RCM combinations (8 total) under the SRES A2 scenario at a spatial resolution of 50 km and has provided the most widely used dynamical projections of 21st century U.S. climate extremes. Where appropriate, findings are supplemented with those from other dynamical and statistical downscaling analyses as well as regional studies.

In this section, we adopt the regional definitions of the recent United States National Climate Assessment (Melillo et al., 2014), whereby the continental United States is subdivided into six regions: the Northwest (WA, OR, ID), the Southwest (CA, NV, UT, AZ, CO, NM), the Great Plains (MT, WY, ND, SD, NE, KS, OK, TX), the Midwest (MN, IA, MO, WI, MI, IL, IN OH), the Southeast (AR, LA, MS, TN, KY, AL, GA, FL SC, NC, VA), and the Northeast (WV, MD, DE, PA, MD, NY, CT, RI, MA, VT, NY, ME). In the following sections, we provide an overview of historical trends in temperature and precipitation extremes as well as an overview of resulting projections based on dynamical and statistical downscaling.

4.1. Historical changes in temperature extremes

Donat et al. (2013) presented trends in extremes for two periods (1901–2010 and 1951–2010) based on the HadEX2 database (a $2.5^\circ \times 3.75^\circ$ gridded dataset of the ETCCDI indicators; Table 1). They report significant (at the 5% level) negative trends in cool nights (TN10p) over nearly the entire contiguous US during both periods of analysis. Significant negative trends in cool days (TX10p) are also reported during both periods of analysis, but primarily for the western US. Significant positive trends in warm nights (TN90p) are reported for the western US for the longer period and for most of the US, except for a region in the Great Plains during the shorter period. Warm days (TX90p) exhibit significant negative trends during both periods over the SE (within the "warming hole" region, see Meehl et al. (2012)) and exhibit significant positive trends only for a few grid points in the west since 1950. Regional studies (e.g., Pryor et al., 2013) have also identified decreases in metrics of summertime maximum temperatures in parts of the Northern Plains and Midwest regions. In the western US (and Great Plains for the longer period of analysis), there is also a significant positive trend in the coldest night (TNn) metric. The coldest day metric shows significant increases only in the extreme northern portion of the NW region for the longer period of analysis. A few grid points in the W and SE have positive significant trends in the warmest night (TNx) during both periods of analysis, while parts of the SE have negative trends in warmest day (TXx), but only for the longer period of analysis.

The analysis of Kunkel et al. (2013b), which was used in the recent National Climate Assessment (Melillo et al., 2014), investigated changes in U.S. extremes by considering the number of 4-day heat waves or cold waves exceeding the 5-year return value computed from station data for 1901–2011. For regions in the eastern United States, the series of warm events is dominated by the 1930s. With the exception of the Southwest region, the trends in heat and cold wave counts were not found to be significant, although most regions have experienced an increase in heat waves and a decrease in cold waves in recent decades. Donat et al. (2013) also considered trends in heat and cold wave metrics (CSDI and WSDI) over the period 1950–2010. In general agreement with Kunkel et al. (2013b), the WSDI was found to be significantly increasing at just a few grid points in the SW and the extreme NE. The CSDI was found to be decreasing significantly over the SW, parts of the Northern Plains, and the extreme NE.

4.2. Historical changes in extreme precipitation

In their analysis of historical trends in the gridded ETCCDI precipitation metrics, Donat et al. (2013) report significant increases in R10 over the southern plains and MW (for their short period of analysis) and significant decreases over one or two grid points in the SW for the long period of analysis. They also report an overwhelmingly positive trend (except for NW) in the contribution from the wettest days (R95ptot), with significant increases in the northern Great Plains and Midwest regions, in accord with the findings of Groisman et al. (2012) and Pryor et al. (2013).

Kunkel et al. (2013b) also considered, again using station-level data, the number of 2-day extreme precipitation events exceeding the 5-year return value for the period of 1901–2011. The trend is positive and significant for the Midwest and Southeast. For a shorter period (1957–2010), Kunkel (2013a) reported that changes were also significant for the Northeast, in accord with other

studies that have reported changes in extreme precipitation in that region (e.g., Groisman et al., 2012; Guilbert et al., 2015). In the past few decades, all regions have experienced greater than normal occurrence of extreme precipitation events as defined above. The regional averages and coarse resolution gridded products used in these studies have the potential to mask important variations in changes in extremes at smaller scales, especially in regions of complex terrain. For example, Madsen and Figdor (2007), Mass et al. (2010), and Rosenberg et al. (2010) report considerable spatial variability in changes in precipitation extremes in the Northwest.

4.3. Projected changes in regional temperature extremes

Kunkel at al. (2013b) presented an analysis of regional temperature projections utilizing the NARCCAP dynamically downscaled data under the SRES A2 scenario. Projections of the change in the annual number of 95 F (35 °C) days (2041–2070 minus 1980–2000) exhibit significant and consistent (among the members) increases over most of the United States, with the largest changes in extreme southern areas where 95 F (35 °C) is near the mean T_{max} during the summer months so a large number of these very warm days already occur. For the same period, NARCCAP models project large decreases (up to 25 days in parts of the Rocky Mountains) in the annual number of days with $T_{min} < 10$ F (-12.2 °C), with significant differences over all regions where such temperatures occur in the current climate. Similarly, the number of days with $T_{min} < 32$ F (0 °C) increases over the contiguous USA, but with the largest changes in the western USA. As a heat-wave metric, Kunkel et al. (2013b) adopted the annual maximum number of consecutive days with $T_{max} > 95$ F (35 °C). NARCCAP projections also indicate significant increases in this metric over nearly the entire United States, but with the largest increases in the Southwest, southern Great Plains and Southeast. Pryor et al. (2013) also used NARCCAP simulations in a study of changes in the Midwest region and identified a marked increase in warm extremes, including a 60% increase in the likelihood of events meeting or exceeding the maximum temperatures observed during the historic 1995 Chicago heat wave.

Diffenbaugh et al. (2005) applied an RCM to the contiguous USA and quantified changes in the frequency of days exceeding the historical 95th percentile T_{max} value and 5th percentile T_{min} value as well as heat waves. They found increases in warm extremes throughout the domain with the largest changes in the Southwest region. They also found decreases in cold extremes everywhere, but greatest in the Great Lakes and NE. Diffenbaugh and Ashfaq (2010) identified summer drying and more anticyclonic circulation in coming decades as the primary drivers of increases in hot extremes throughout much of the United States.

Regional statistical downscaling studies have also focused on extremes. For example Ahmed et al. (2013) and Ning et al. (2015) applied variations of bias correction and spatial disaggregation (BCSD, where GCM bias is corrected at coarse resolution and then applied to observational data that are at higher resolution than the model's grid) to the Northeast region and investigated changes in several ETCCDI indicators. Both studies highlighted increases in warm extremes and decreases in cold extremes throughout the region. Ahmed et al. (2013) found greater agreement among models after bias correction and also noted that use of dynamical downscaling as an intermediate step had little effect on the results. Ning et al. (2015) also show a projected increase in the interannual variability temperature and precipitation extremes.

4.4. Projected changes in regional precipitation extremes

NARCCAP simulations have been widely used to investigate future precipitation extremes, with the results highlighted here referring to mid-late 21st century conditions (unless otherwise noted). Kunkel et al. (2013b) found increases in the number of precipitation events greater than 1 in. (25.4 mm) over much of the US with the greatest agreement (among NARCCAP models) in the Rocky Mountains, northern Great Plains, upper Midwest, and Northeast regions. Wehner (2013b) reports similar results using NARCCAP models with EVT. Similarly, Halmstad et al. (2013) applied quantile mapping and EVT to NARCCAP output for the Willamette River Basin in the Northwest region and found increases in the 2- and 25-year return value for precipitation for 2038–2069. Pryor et al. (2013) used NARCCAP simulations and reported increases in RX5day and total precipitation on the 10 wettest days of the year increasing by 10% for the Midwest region. Dominguez et al. (2012) also combined NARCCAP projections and EVT and reported increasing extremes in wintertime precipitation in the western USA (12.6% increase in the 20-year return period precipitation and 14.4% increase in the 50-year return period daily precipitation), even in areas where the mean seasonal precipitation is likely to decrease. Using the RegCM3 regional climate model, Diffenbaugh et al. (2005) also projected increases in the frequency of precipitation events exceeding the 95th percentile reference integration (1961–1985) value, as well as changes in the fraction of precipitation resulting from extreme events, in many US regions.

Statistical downscaling has also been widely used to develop projections of regional precipitation extremes. Schoof (2015) applied a statistical downscaling technique described by Wilks (1999) to CMIP5 models and the 0.25° Climate Prediction Center precipitation analysis and used ETCCDI indicators derived from time series generated using a stochastic weather model to investigate possible changes in regional precipitation extremes. Under high levels of forcing from greenhouses gases (RCP 8.5), the maximum 1-day precipitation total (RX1day) as well as the number of heavy (10 mm; R10) and very heavy (20 mm; R20) events increased significantly over most of the contiguous United States with the exception of the Southwest and parts of the extreme south. Ning et al. (2015) used statistical downscaling (BCSD) and found increases in extreme precipitation in the Northeast region under all levels of greenhouse gas forcing (2050–2099 vs. 1950–1999), but like Schoof (2015), reported greater increases under higher forcing. Tryhorn and DeGaetano (2011) utilized multiple statistical downscaling approaches with EVT to derive projections of extreme precipitation in the Northeast region, finding consistent but regionally varying increases in extreme precipitation for the 2041–2060 period under the SRES A2 scenario. Lastly, Wang and Zhang (2008) applied EVT to downscaled 2050–99 output from a single climate model (CCCma CGCM3.1) and found increases in extreme precipitation risk based on the 20-year return value over much of the United States.

5. Examples of regional downscaling of temperature extremes in the U.S.

In this section, examples of regional climate downscaling for the analysis of extremes are developed by applying quantile mapping to the newly available daily PRISM (Parameter–elevation Relationships on Independent Slopes; Daly et al., 2008) data, available from www.prism.oregonstate.edu. The daily PRISM data are available starting in 1981 and are derived from climatologically-aided interpolation (Willmott and Robeson, 1995) of station data. The resulting data set has more than 480,000 grid points covering the contiguous USA at a resolution of approximately 4 km. For the purposes of this work, we analyze the grid points within a $3° \times 4°$ box from each of the six regions of the contiguous

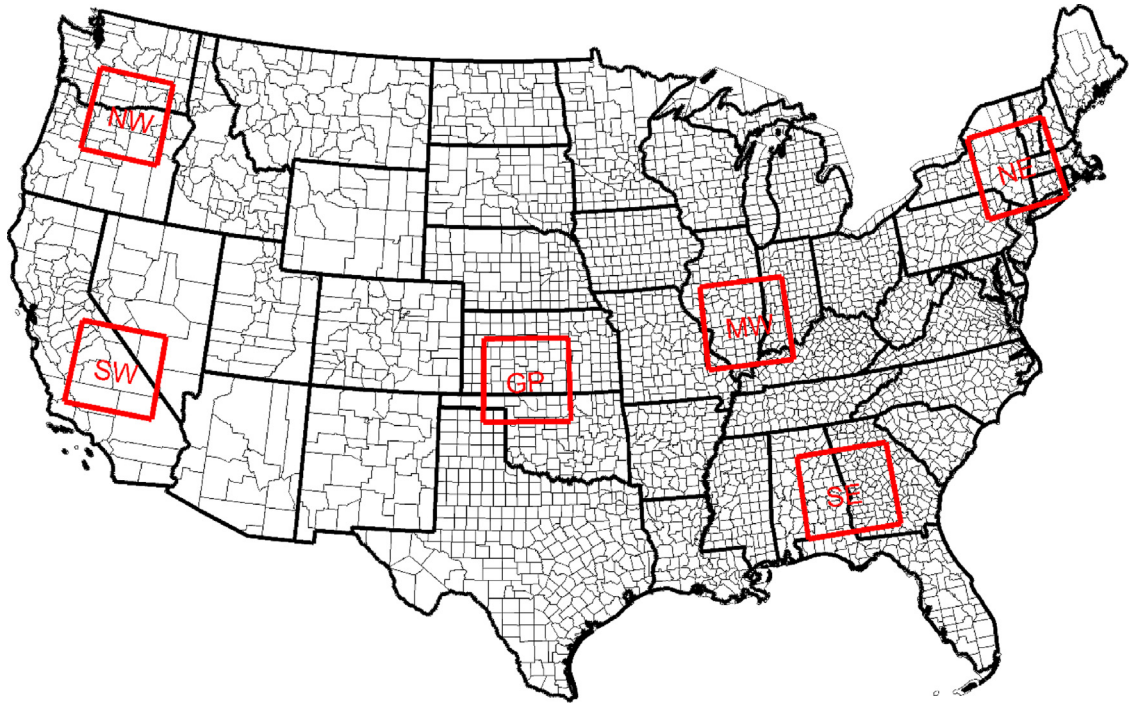

Fig. 1. Map of the United States showing the 3° × 4° boxes used for regional-scale projections. Within each region, daily temperature output for eight CMIP5 models (using the RCP8.5 scenario) was bias corrected and downscaled to the PRISM grid for 1981–2005 and 2071–2095. Labels indicate the regions referred to in Section 4: Northwest (NW), Southwest (SW), Great Plains (GP), Midwest (MW), Northeast (NE) and Southeast (SE). The dark lines represent state boundaries and the light lines are county boundaries.

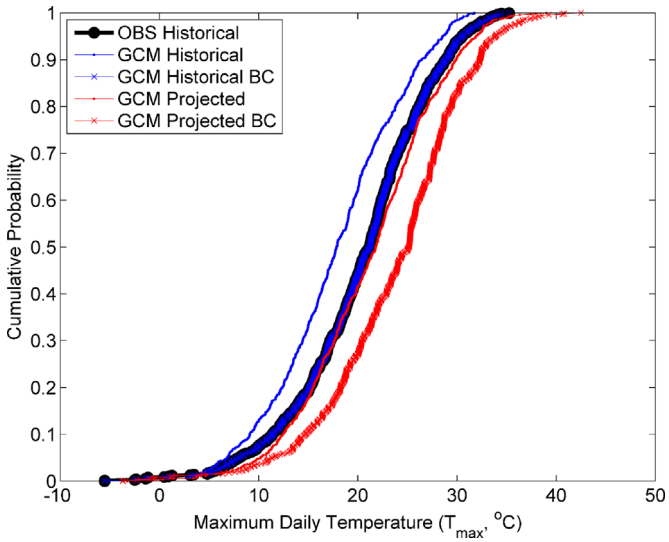

Fig. 2. Demonstration of the quantile mapping approach used for bias correction (BC) for 38.9791°N, 100.4375°W during October. A distinct bias correction is applied for each location and month. The black line represents the location- and month-specific historical cumulative distribution function (ECDF) for T_{max} from the historical (PRISM) data. The thin blue line represents the CDF from the co-located GCM grid box over the same time period. Quantile mapping corrects the GCM-derived CDF so that it matches the observed CDF. The corrected CDF is shown by the thick blue line. Finally, quantiles derived from the future GCM simulation (thin red line) are adjusted by the same amount as the quantiles from the historical period to derive the bias-corrected future GCM simulation (thick red line). (For interpretation of the references to color in this figure legend, the reader is referred to the web version of this article.)

United States described in Section 4 (Fig. 1). Our analysis focuses on daily maximum and minimum temperature (T_{max}, T_{min}) data from 8 CMIP5 models BCC-CSM1.1 (Xin et al., 2012), BNU-ESM (Ji et al., 2014,), Can-ESM2 (Arora et al., 2011; von Salzen et al., 2013), GFDL-CM3 (Donner et al., 2011) IPSL-CM5A-LR (Dufresne et al., 2012), MPI-ESM-LR (Stevens et al., 2013), MRI-CGCM3 (Yukimoto et al., 2012), and NorESM1-M (Bentsen et al., 2013). Each model's output was bias-corrected using quantile-mapping of the model's 1981–2005 ecdf to that of the high-resolution PRISM grid, with the biases estimated from 1981–2005 then being applied to the corresponding quantiles for 2071–2095 (e.g., Fig. 2) under the RCP8.5 pathway (see Moss et al. (2010)). Following bias correction, a subset of the ETCCDI indicators was computed at high resolution, with maps and summary statistics for each of the regions being used to show projected changes.

5.1. Changes in threshold-based ETCCDI temperature indicators

The bias-corrected results for threshold-based temperature

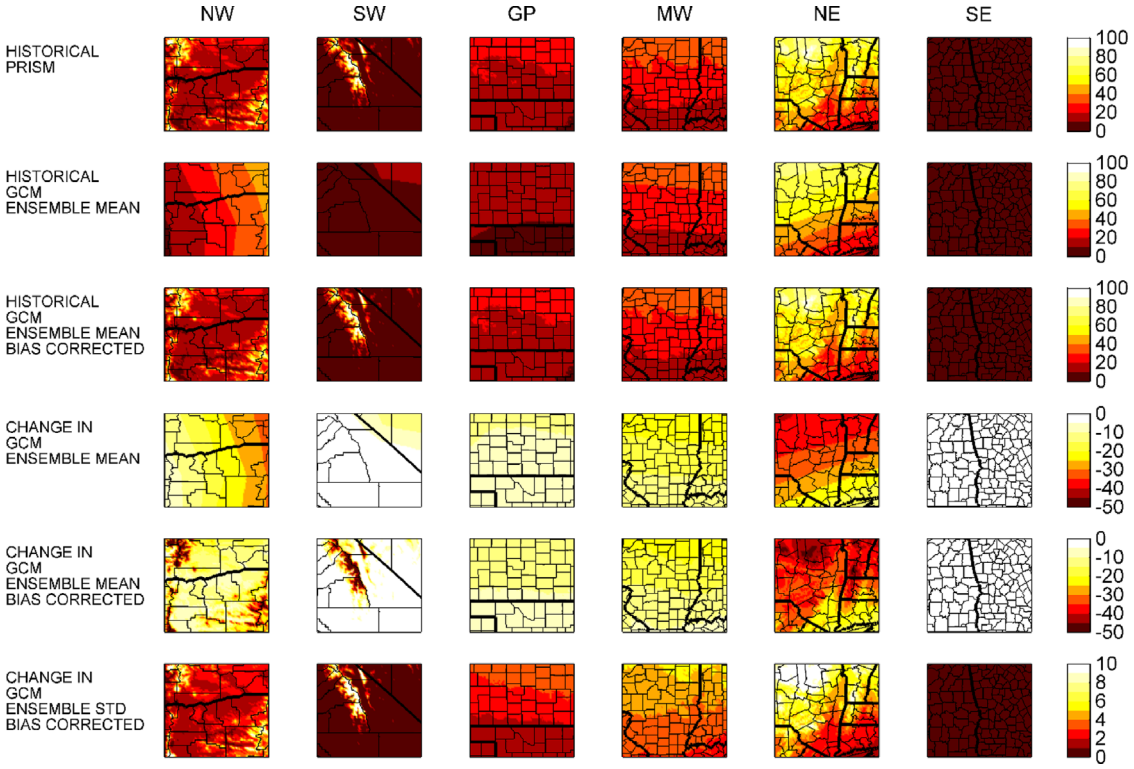

Fig. 3. Observed and projected values of the icing days ETCCDI indicator. The annual mean of the PRISM values for 1981–2005 are shown in the first row, followed by the multi-model mean for the same period without (2nd row) and with (3rd row) bias correction using quantile mapping, the difference of the multi-model mean of the projected changes (2071–2095) minus those of the 1981–2005 period without (4th row) and with (5th row) bias correction using quantile mapping, and the multi-model standard deviation of the projected changes in the final row. The regions are as shown in Fig. 1. The dark lines represent state boundaries and the light lines are county boundaries.

extreme indicators are presented in Fig. 3 through 6, with regional statistics presented in Table 2. Some of the threshold-based indicators, such as icing days (ID; days with $T_{max} < 0$ °C; Fig. 3) are relatively rare in some regions, so it's clear that not all ETCCDI indicators are applicable to all regions. At the same time, the fine spatial resolution of the results – particularly in regions with larger relief – clearly demonstrates the utility of the downscaling approach for estimating extremes. In addition, the bias correction is an essential step in developing realistic values of the indicators for both the historical and projection periods in some regions. Below, we highlight a few of the key results of the downscaling and projections across the regions.

Historical statistics derived from the PRISM data for the subregions indicate the largest number of icing days occurs in the NE region, but with substantial spatial variability within the Northwest and Southwest regions where large temperature variations exist due to topography (Fig. 3). For the downscaled projections, all regions exhibit decreases in icing days under the RCP8.5 pathway. While there is some variability among the GCMs used, the ensemble standard deviation is small relative to the projected change (Fig. 3, Table 2). The largest changes occur in areas that currently have large number of icing days, such as high elevations of the Northwest and Southwest regions and northern portions of the Northeast region. The downscaled results presented here indicate fewer frost days across all GCMs and all grid points in each region (Fig. 4, Table 2). Like icing days, the largest changes in frost days correspond to regions with the largest historical counts. The variation among GCMs is small (approximately 20%) relative to the change in the ensemble mean for each region (Table 2).

The historical counts of tropical nights (TR; days with $T_{min} > 20$ °C) and summer days (SU; days with $T_{max} > 25$ °C) are highest in the Southeast region and in the low elevations of the Southwest region (Fig. 5, Table 2). Projected changes in TR and SU are positive over all grid points in all regions for all of the GCMs considered. Many regions are projected to experience counts of TR that are more than twice as large as the historical ones (Table 2). Despite large regional differences in SU during the historical period, regionally-averaged changes are similar and range from 47.3 days in the Northwest region to 65.6 days in the Northeast region. For most regions (excepting the Northwest and Northeast regions for TR), the ensemble standard deviation is around 20% of the ensemble mean projected change for the TR and SU metrics (Table 2). The fine-scale spatial variability produced by the downscaling procedure is most pronounced in the maps of ensemble mean differences of TR and SU for the NW and SW, where the temperature-elevation impacts of the Cascade volcanoes and the high Sierras are clearly evident (Fig. 6). But even regions such as the Great Plains and Midwest, that are usually considered to be relatively homogeneous, show within-region differences of projected changes in SU that are greater than 10 days within the $3° \times 4°$ areas.

5.2. Changes in percentile-based ETCCDI temperature indicators

While threshold-based indicators of extremes exhibit large geographical variations (Figs. 7 and 8, Table 2), percentile-based approaches allow quantification of change relative to the local climate. By definition, all grid points have 10% of the historical record higher than the 90th percentile T_{max} and T_{min} values (TX90p, TN90p) and 10% lower than the 10th percentile T_{max} and T_{min} values (TX10p, TN10p).

Changes in the percentile-based cold extremes are shown in

Table 2
Regionally-averaged values and changes for the threshold-based extreme temperature indicators. For each indicator and region, values are provided for the historical regional mean from 1981–2005, the historical regional mean based on an 8 model ensemble, the historical regional mean based on an eight model ensemble with bias correction via quantile mapping, difference of the regional mean of the 8 downscaled GCMs for 2071–2095 from that of the 1981–2005 mean with and without bias correct via quantile mapping, and the standard deviation (consistency) of the projected mean change across the 8 downscaled GCMs. All units are in days/year.

	NW	SW	GP	MW	NE	SE
Icing Days (*ID*)						
Historical: PRISM	22.1	6.5	16.9	24.7	48.6	0.8
Historical: GCM Mean	26.6	3.0	11.8	25.1	48.9	0.8
Historical: GCM Mean Bias Corrected	22.0	6.5	16.8	24.6	48.5	0.8
Change: GCM Mean	−19.9	−2.7	−8.4	−17.5	−30.6	−0.7
Change: GCM Mean Bias Corrected	−16.9	−4.7	−10.1	−15.7	−32.6	−0.5
Change: GCM STD Bias Corrected	2.5	0.7	2.3	4.0	5.3	0.2
Frost Days (*FD*)						
Historical: PRISM	139.9	86.6	118.0	108.1	155.9	45.1
Historical: GCM Mean	105.6	49.6	76.1	87.1	112.5	23.9
Historical: GCM Mean Bias Corrected	139.8	86.5	117.8	107.9	155.7	45.0
Change: GCM Mean	−63.0	−35.4	−41.0	−42.0	−49.0	−15.0
Change: GCM Mean Bias Corrected	−79.9	−40.6	−47.7	−47.4	−57.8	−26.9
Change: GCM STD Bias Corrected	17.3	7.3	9.6	8.6	9.5	5.2
Tropical Nights (*TN*)						
Historical: PRISM	0.4	22.0	32.9	28.2	3.1	66.8
Historical: GCM Mean	0.1	13.2	60.6	58.1	17.8	105.0
Historical: GCM Mean Bias Corrected	0.4	22.0	32.9	28.2	3.1	66.7
Change: GCM Mean	13.0	50.5	62.0	64.6	63.3	69.0
Change: GCM Mean Bias Corrected	15.3	45.8	66.9	67.7	36.0	68.6
Change: GCM STD Bias Corrected	8.1	9.4	12.0	12.9	13.2	11.1
Summer Days (*SU*)						
Historical Mean	72.6	140.2	147.2	127.5	63.8	188.5
Historical: GCM Mean	42.2	114.3	129.0	115.6	50.4	161.3
Historical: GCM Mean Bias Corrected	72.6	140.2	147.2	127.5	63.7	188.4
Change: GCM Mean	49.2	47.5	51.4	50.9	69.1	55.8
Change: GCM Mean Bias Corrected	47.3	47.7	50.0	49.6	65.6	52.7
Change: GCM STD Bias Corrected	9.7	10.5	9.2	10.9	12.1	11.9

Fig. 7 and Table 3. All of the regions considered are projected to experience substantive reductions in the number of days falling below the 10th percentile historical T_{max} and T_{min} values, with larger changes for T_{min} than T_{max} in each region (Fig. 7, Table 3). For both TN10p and TX10p, the largest changes are projected for the Northeast region, where the temperatures that were the 10th percentile during 1981–2005 occur on less than 1% of days during 2071–2095. The smallest changes are projected for the Great Plains, with a reduction to 2–3% of days having the historical 10th percentile temperature values. As with the threshold-based indicators, the standard deviations of the regional averages are much smaller than the projected changes, reflecting a strong signal relative to variations among the GCMs used.

Large increases are also projected for percentile-based warm extremes (TN90p, TX90p; Fig. 7, Table 3). In all of the regions considered, an average of at least 40% of days during the 2071–2095 period are projected to have T_{max} and T_{min} values that exceed the historical 90th percentile values. In the Southeast region, at least 50% of the days meet the 90th percentile criteria for both T_{max} and T_{min}. These changes are also accompanied by relatively small standard deviations among the GCM used (Table 3).

6. Summary and recommendations

In this paper, we have reviewed metrics for estimating temperature and precipitation extremes, as well as the methodological approaches for developing projections of regional climate extremes. We have also reviewed the findings of studies that have developed projections of temperature and precipitation extremes for US regions. Using a high-resolution observational dataset (PRISM) for a number of US sub-regions, we presented bias-corrected and downscaled projections of temperature extremes for a late-century period under strong greenhouse gas forcing (RCP 8.5). Many regions have already experienced statistically significant increases in extreme events, with a widespread decrease in cool nights (TN10p) and regional changes (both warming and cooling) in daytime temperatures and in the fraction of precipitation derived from intense events. Future projections are less ambiguous with large decreases in cold extremes, increases in warm extremes, and changes in the character of precipitation across regions. For the 2071–2095 timeframe considered here and elsewhere, GCMs and emissions scenarios are the primary sources of uncertainty (Hawkins and Sutton, 2009). While just a single emissions pathway was considered (RCP8.5) in our regional downscaling approach, this is the RCP that current emissions are mostly closely tracking (Sanford et al., 2014). In addition, the magnitude of model differences relative to ensemble mean changes reflects a strong signal to noise ratio among the GCMs.

Studies of changes in extremes have traditionally focused on larger regions and/or coarser resolution than those considered in the demonstration presented here (Section 5). As shown in Fig. 3 through 8, substantial spatial variability in extremes and their changes is presented at the sub-regional scale, even within regions that often are considered relatively homogeneous. The impacts of changes in extremes are unlikely to be uniform across even small geographic areas. The impacts are also likely to depend on how changes are distributed across seasons, which, due to space constraints, have not been considered here. It is also important to note that the availability of high resolution observational data still presents a major limitation for this type of analysis in many parts of the world.

Impacts of climate extremes often result from simultaneous extremes in more than one variable. For that reason, an emerging theme in the analysis of extremes is bivariate or multivariate extremes (AghaKouchak et al., 2014; Schoelzel and Friederichs, 2008). For example, understanding the influence of climate extremes on agricultural yield requires consideration of both growing season temperature and precipitation extremes. For human health considerations, prolonged periods with extreme temperatures and humidity are an important consideration. Often, application-dependent criteria are needed to translate changes in climate extremes to changes in impacts. As noted by Kunkel et al. (2013a), detecting or projecting changes in extremes is only the first step toward mitigating their impact.

Research on changes in regional extremes is likely to produce “actionable” results for mitigation of impacts in the next decade, requiring careful consideration of uncertainty and presentation of results in terms that are understood by stakeholders (Pidgeon and Fischoff, 2011). For example, Rosenberg et al. (2010) used the Weather Research and Forecasting (WRF) regional model to downscale precipitation from two GCMs (using different GHG forcing) in the Northwest and found an increase in extreme events, but found that the range of results was too large to inform engineering design. Understanding the differences in projections developed using different GCMs, downscaling tools, and

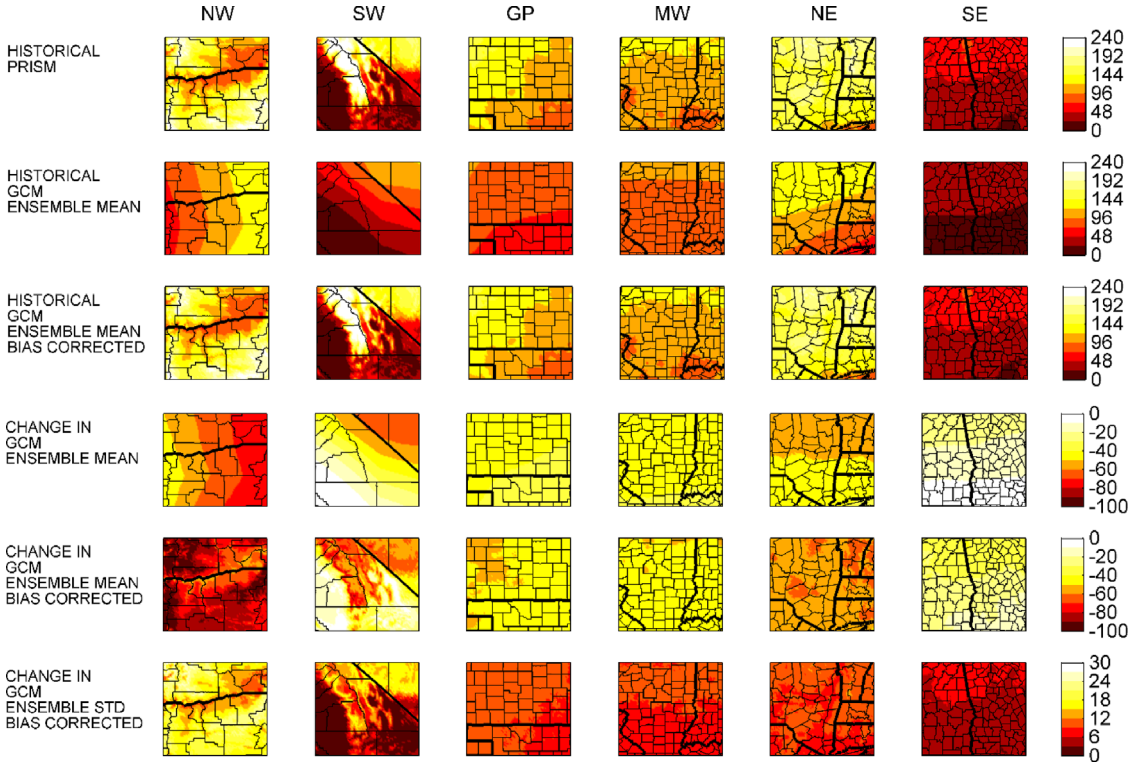

Fig. 4. Observed and projected values of the frost days ETCCDI indicator. The annual mean of the PRISM values for 1981–2005 are shown in the first row, followed by the multi-model mean for the same period without (2nd row) and with (3rd row) bias correction using quantile mapping, the difference of the multi-model mean of the projected changes (2071–2095) minus those of the 1981–2005 period without (4th row) and with (5th row) bias correction using quantile mapping, and the multi-model standard deviation of the projected changes in the final row. The regions are as shown in Fig. 1. The dark lines represent state boundaries and the light lines are county boundaries.

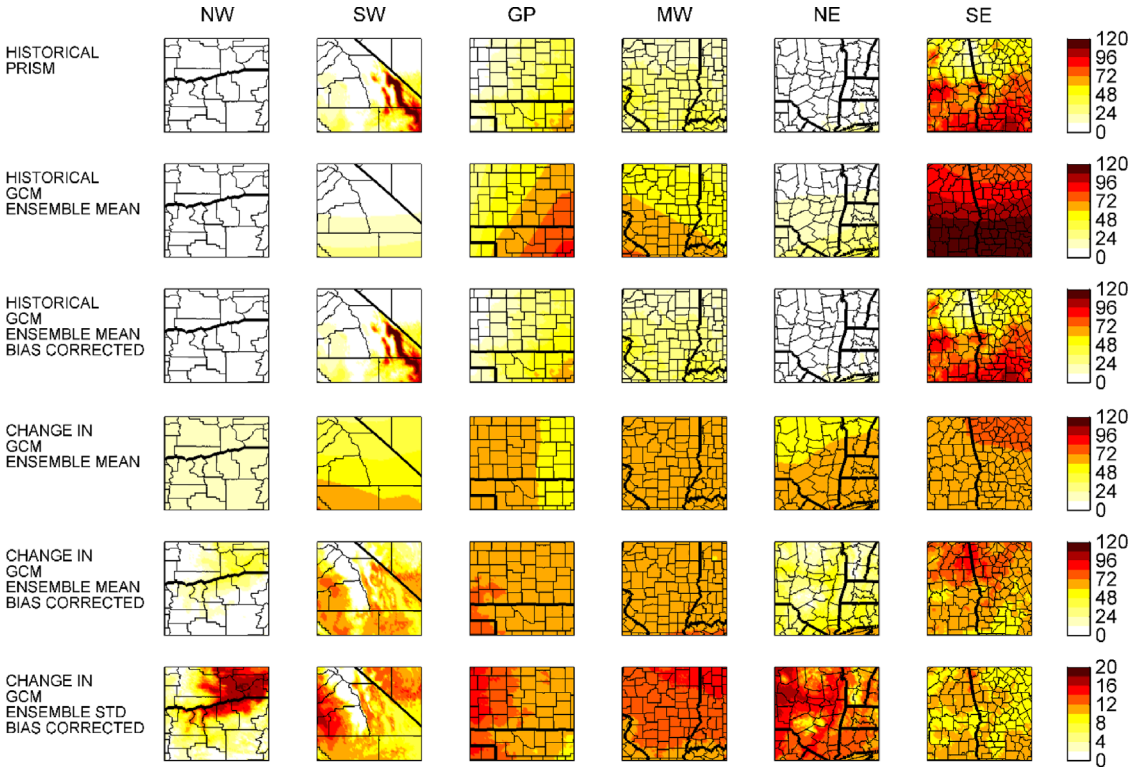

Fig. 5. Observed and projected values of the tropical nights ETCCDI indicator. The annual mean of the PRISM values for 1981–2005 are shown in the first row, followed by the multi-model mean for the same period without (2nd row) and with (3rd row) bias correction using quantile mapping, the difference of the multi-model mean of the projected changes (2071–2095) minus those of the 1981–2005 period without (4th row) and with (5th row) bias correction using quantile mapping, and the multi-model standard deviation of the projected changes in the final row. The regions are as shown in Fig. 1. The dark lines represent state boundaries and the light lines are county boundaries.

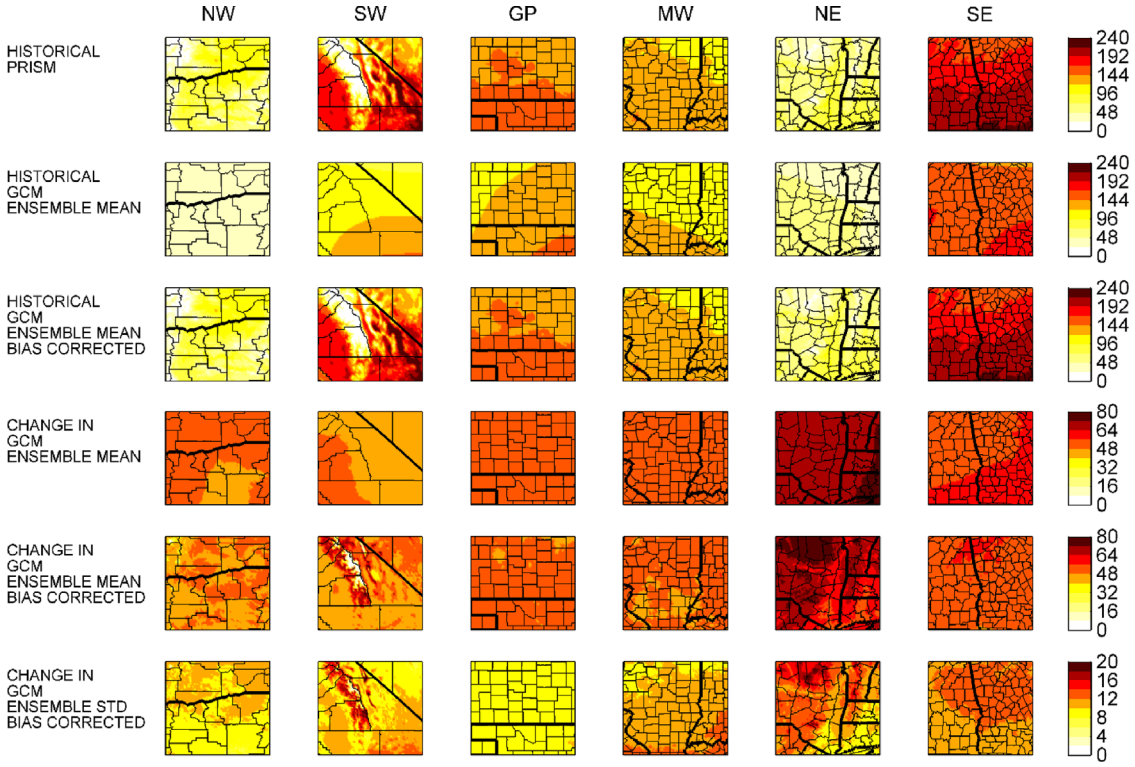

Fig. 6. Observed and projected values of the summer days ETCCDI indicator. The annual mean of the PRISM values for 1981–2005 are shown in the first row, followed by the multi-model mean for the same period without (2nd row) and with (3rd row) bias correction using quantile mapping, the difference of the multi-model mean of the projected changes (2071–2095) minus those of the 1981–2005 period without (4th row) and with (5th row) bias correction using quantile mapping, and the multi-model standard deviation of the projected changes in the final row. The regions are as shown in Fig. 1. The dark lines represent state boundaries and the light lines are county boundaries.

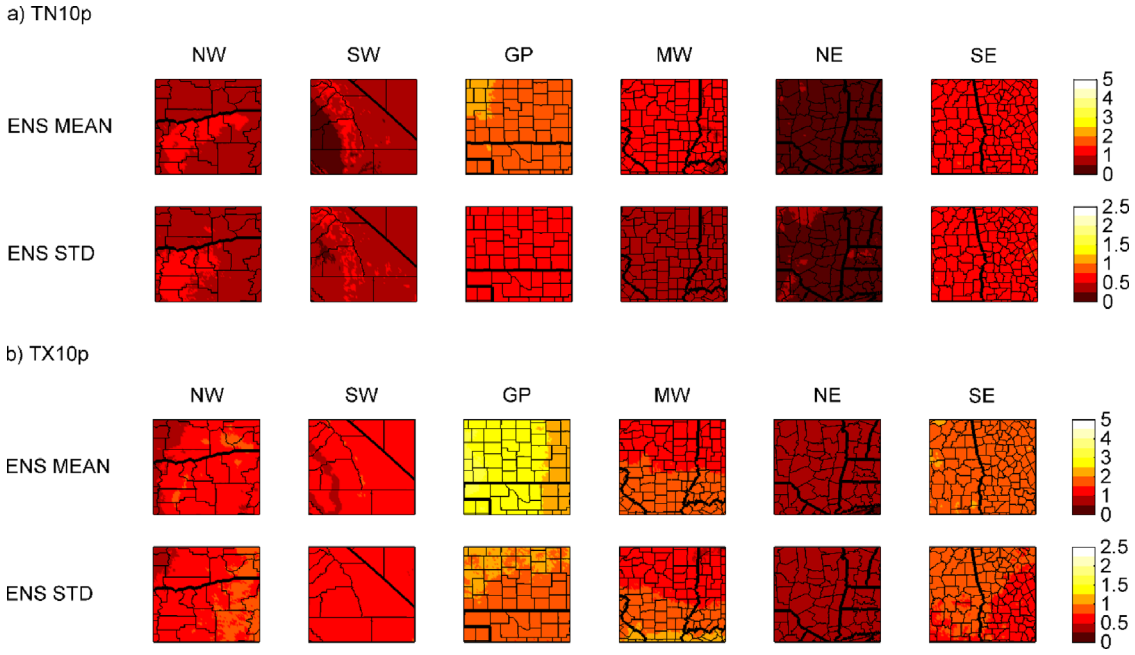

Fig. 7. Projected values of the cold extremes using percentile-based ETCCDI indicators. For each indicator, the first row of maps shows the multi-model mean for 2071–2095 and the second row of maps indicates the ensemble standard deviation for period 2071–2095 (in percent). The regions are as shown in Fig. 1. The dark lines represent state boundaries and the light lines are county boundaries.

definitions for extremes, will reduce the range and uncertainty of estimated changes by identifying unrealistic or inappropriate methods. Key to this process is the identification of physical mechanisms leading to changes in extremes, including their seasonal variations (Gutowski et al., 2010; Trenberth et al., 2015). For example, extreme precipitation events in the United States are typically associated with extratropical cyclones, tropical cyclones, mesoscale convective systems, monsoon events, and associated teleconnections with sea-surface temperature (Kunkel et al., 2013a), but processes across spatial scales, including soil moisture

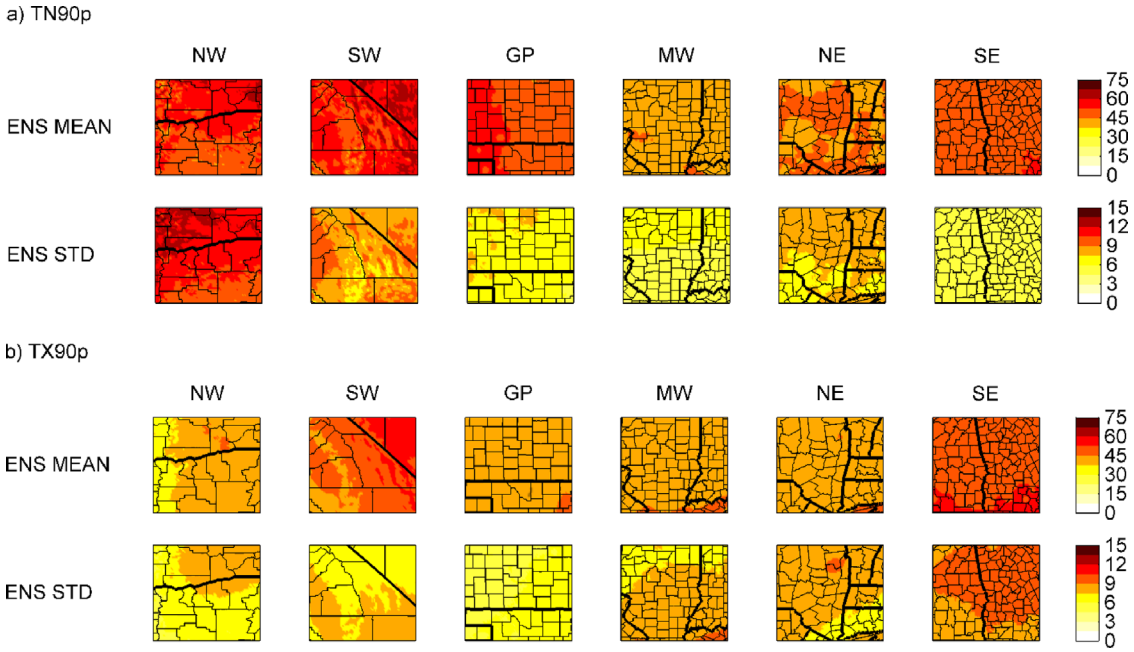

Fig. 8. Projected values of the warm extremes using percentile-based ETCCDI indicators. For each indicator, the first row of maps shows the multi-model mean for 2071–2095 and the second row of maps indicates the ensemble standard deviation for period 2071–2095 (in percent). The regions are as shown in Fig. 1. The dark lines represent state boundaries and the light lines are county boundaries.

Table 3
Regionally-averaged values for the percentile-based extreme temperature indicators. For each indicator and region, values are percentages for the projected 2071–2095 mean percentage for 2071–2095 among the 8 downscaled GCMs and the standard deviation of the mean projected percentage among the 8 downscaled GCMs. All units are in percentages of days.

	NW	SW	GP	MW	NE	SE
TN10p						
Ensemble Mean	0.9	0.7	1.9	1.1	0.4	1.3
Ensemble STD	0.5	0.4	0.6	0.4	0.2	0.7
TX10p						
Ensemble Mean	1.2	1.2	2.7	1.5	0.6	1.9
Ensemble STD	0.7	0.6	0.9	0.8	0.4	0.8
TN90p						
Ensemble Mean	53.5	55.1	51.1	43.6	45.5	50.0
Ensemble STD	11.2	8.5	7.1	5.8	7.8	5.2
TX90p						
Ensemble Mean	40.0	49.1	41.1	43.1	42.3	51.1
Ensemble STD	7.1	7.4	6.1	7.9	8.1	9.1

(Durre et al., 2000), evapotranspiration (Diffenbaugh et al., 2005), land cover (Deo et al., 2009) and even loss or reconfiguration of sea-ice at high latitudes (Tang et al., 2013), often work in concert to produce regional extreme events. For example, Kenyon and Hegerl (2010) examined precipitation extremes as they relate to large scale modes of atmospheric circulation variability and Grotjahn et al. (2015) have reviewed short duration temperature extremes in North America with special attention given to the corresponding large scale meteorological patterns. Evaluation of climate model simulations in the context of these multi-scale processes and their relation to regional extremes (as in Loikith et al. (2015)) should be a key focus for the next decade of research.

Acknowledgments

This material is partially based upon work supported by the National Science Foundation under grant 1009925. Any opinions, findings, and conclusions or recommendations expressed in this material are those of the authors and do not necessarily reflect the views of the National Science Foundation. We acknowledge the World Climate Research Programme's Working Group on Coupled Modeling, which is responsible for CMIP, and thank the climate modeling groups (listed in Section 2) for producing and making available their model output. For CMIP, the U.S. Department of Energy's Program for Climate Model Diagnosis and Intercomparison provided coordinating support and led the development of software infrastructure in partnership with the Global Organization for Earth System Science Portals. We also acknowledge the provision of the PRISM data from the PRISM research group at Oregon State University, http://prism.oregonstate.edu.

References

Abatzoglou, J.T., Brown, T.J., 2012. A comparison of statistical downscaling methods suited for wildfire applications. Int. J. Climatol. 32, 772–780.

AghaKouchak, A., Cheng, L., Mazdiyasni, O., Farahmand, A., 2014. Global warming and changes in risk of concurrent climate extremes: insights from the 2014 California drought. Geophys. Res. Lett. 41, 8847–8852. http://dx.doi.org/10.1002/2014GL062308.

Ahmed, K.Z., Wang, G., Silander, J., Wilson, A.M., Allen, J.M., Horton, R., Anyah, R., 2013. Statistical downscaling and bias correction of climate model outputs for climate change impact assessment in the U.S. northeast. Glob. Planet. Chang. 100, 320–332.

Alexander, L.V., Zhang, X., Peterson, T.C., Caesar, J., Gleason, B., Klein Tank, A.M.G., Haylock, M., Collins, D., Trewin, B., Rahimzadeh, F., Tagipour, A., Rupa Kumar, K., Revadekar, J., Griffiths, G., Vincent, L., Stephenson, D.B., Burn, J., Aguilar, E., Brunet, M., Taylor, M., New, M., Zhai, P., Rusticucci, M., Vazquez-Aguirre, J.L., 2006. Global observed changes in daily climate extremes of temperature and precipitation. J. Geophys. Res. 111, D05109. http://dx.doi.org/10.1029/2005JD006290.

Anyamba, A., Small, J.L., Britch, S.C., Tucker, C.J., Pak, E.W., et al., 2014. Recent weather extremes and impacts on agricultural production and vector-borne disease outbreak patterns. PLoS One 9, e92538. http://dx.doi.org/10.1371/journal.pone.0092538.

Arora, V.K., Scinocca, J.F., Boer, G.J., Christian, J.R., Denman, K.L., Flato, G.M., Kharin, V.V., Lee, W.G., Merryfield, W.F., 2011. Carbon emission limits required to satisfy future representative concentration pathways of greenhouse gases. Geophys. Res. Lett. 38, L05805. http://dx.doi.org/10.1029/2010GL046270.

Bentsen, M., Bethke, I., Debernard, J.B., Iversen, T., Kirkevag, A., Seland, O., Drange, H., Roelandt, C., Seierstad, I.A., Hoose, C., Kristjansson, J.E., 2013. The Norwegian Earth System Model, NorESM1-M – Part I: Description and basic evaluation of the physical climate. Geosci. Model Dev. 6, 687–720. http://dx.doi.org/10.5194/

gmd-6-687-2013.
Brown, S.J., Caesar, J., Ferro, C.A.T., 2008. Global changes in extreme daily temperature since 1950. J. Geophys. Res. 113, D05155. http://dx.doi.org/10.1029/2006JD008091.
Cheng, L., AghaKouchak, A., Gilleland, E., Katz, R.W., 2014. Non-stationary extreme value analysis in a changing climate. Clim. Chang. 127, 353–369.
Christidis, N., Stott, P.A., Brown, S.J., 2011. The role of human activity in the recent warming of extremely warm daytime temperatures. J. Clim. 24, 1922–1930. http://dx.doi.org/10.1175/2011JCLI4150.1.
Coles, S.G., 2001. An Introduction to Statistical Modeling of Extreme Values. Springer, Berlin, Heildelberg, p. 225 (Springer Series in Statistics).
Collins, M., Knutti, R., Arblaster, J., Dufresne, J.-L., Fichefet, T., Friedlingstein, P., Gao, X., Gutowski, W.J., Johns, T., Krinner, G., Shongwe, M., Tebaldi, C., Weaver, A.J., Wehner, M., 2013. Long-term climate change: projections, commitments and irreversibility. In: Stocker, T.F., Qin, D., Plattner, G.-K., Tignor, M., Allen, S.K., Boschung, J., Nauels, J., Xia, Y., Bex, V., Midgley, P.M. (Eds.), *Climate* Change 2013: The Physical Science Basis. Contribution of Working Group I to the Fifth Assessment Report of the Intergovernmental Panel on Climate Change. Cambridge University Press, Cambridge, United Kingdom and New York, NY, USA.
Daly, C., Halbleib, M., Smith, J., Gibson, W.P., Doggett, M.K., Taylor, G.H., Curtis, J., Pasteris, P.P., 2008. Physiographically sensitive mapping of climatological temperature and precipitation across the conterminous United States. Int. J. Climatol. 28, 2031–2064.
Deo, R.C., Syktus, J.I., McAlpine, C.A., Lawrence, P.J., McGowan, H.A., Phinn, S.R., 2009. Impact of historical land cover change on daily indices of climate extremes including droughts in eastern Australia. Geophys. Res. Lett. 36, L08705. http://dx.doi.org/10.1029/2009GL037666.
Diffenbaugh, N.S., Pal, J.S., Trapp, R.J., Giorgi, F., 2005. Fine-scale processes regulate the response of extreme events to global climate change. Proc. Natl. Acad. Sci. 102, 15774–15778. http://dx.doi.org/10.1073/pnas.0506042102.
Diffenbaugh, N.S., Ashfaq, M., 2010. Intensification of hot extremes in the United States. Geophys. Res. Lett. 37, L15701. http://dx.doi.org/10.1029/2010GL043888.
Dominguez, F., Rivera, E., Lettenmaier, D.P., Castro, C.L., 2012. Changes in winter precipitation extremes for the western United States under a warmer climate as simulated by regional climate models. Geophys. Res. Lett. 39, L05803. http://dx.doi.org/10.1029/2011GL050762.
Donat, M.G., Alexander, L.V., Yang, H., Durre, I., Vose, R., Dunn, R.J.H., Willett, K.M., Aguilar, E., Brunet, M., Caesar, J., Hewitson, B., Jack, C., Klein Tank, A.M.C., Kruget, A.C., Marengo, J., Peterson, T.C., Renom, M., Oria Rojas, C., Rusticucci, M., Salinger, J., Elrayah, A.S., Sekele, S.S., Srinivasta, A.K., Trewin, B., Villarroel, C., Vincent, L.A., Zhai, P., Zhang, X., Kitching, S., 2013. Updated analyses of temperature and precipitation extreme indices since the beginning of the twentieth century: the HadEX2 dataset. J. Geophys. Res.: Atmos. 118, 2098–2118. http://dx.doi.org/10.1002/jgrd.50150.
Donner, L.J., Wyman, B., Hemler, R.S., Horowitz, L., Ming, Y., Zhao, M., Golaz, J.-C., Ginoux, P., Lin, S.-J., Schwarzkopf, M.D., Austin, J., Alaka, G., Cooke, W.F., Delworth, T.L., Freidenreich, S., Gordon, C.T., Griffies, S., Held, I., Hurlin, W.J., Klein, S.A., Knutson, T.R., Langenhorst, A.R., Lee, H.C., Lin, Y., Magi, B.I., Malyshev, S., Naik, V., Nath, M.J., Pincus, R., Ploshay, J.J., Ramaswamy, V., Seman, C.J., Shevliakova, E., Sirutis, J.J., Stern, W.F., Stouffer, R.J., Wilson, R.J., Winton, M., Wittenberg, A.T., Zeng, F., 2011. The dynamical core, physical parameterizations, and basic simulation characteristics of the atmospheric component AM3 of the GFDL Global Coupled Model CM3. J. Clim. 24, 3484–3519. http://dx.doi.org/10.1175/2011JCLI3955.1.
Dufresne, J.-L., Foujols, M.-A., Denvil, S., Caubel, A., Marti, O., Aumont, O., Balkanski, Y., Bekki, S., Bellenger, H., Benshila, R., Bony, S., Bopp, L., Braconnot, P., Brockmann, P., Cadule, P., Cheruy, F., Codron, F., Cozic, A., Cugnet, D., de Noblet, N., Duvel, J.-P., Ethe, C., Fairhead, L., Fichefet, T., Flavoni, S., Friedlingstein, P., Grandpeix, J.-Y., Guez, L., Guilyardi, E., Hauglustaine, D., Hourdin, F., Idelkadi, A., Ghattas, J., Joussaume, S., Kageyama, M., Krinner, G., Labetoulle, S., Lahellec, A., Lefebvre, M.-P., Lefevre, F., Levy, C., Li, Z.X., Lloyd, J., Lott, F., Madec, G., Mancip, M., Marchand, M., Masson, S., Meurdesoif, Y., Mignot, J., Musat, I., Parouty, S., Polcher, J., Rio, C., Schulz, M., Swingedouw, D., Szopa, S., Talandier, C., Terray, P., Viovy, N., Vuichard, N., 2012. Climate change projections using the IPSL-CM5 Earth System Model: from CMIP3 to CMIP5. Clim. Dyn. 40, 2123–2165. http://dx.doi.org/10.1007/s00382-012-1636-1.
Durre, I., Wallace, J.M., Lettenmaier, E.P., 2000. Dependence of extreme daily maximum temperatures on antecedent soil moisture in the contiguous United States during summer. J. Clim. 13, 2461–2651.
Emori, S., Brown, S.J., 2005. Dynamic and thermodynamic changes in mean and extreme precipitation under changed climate. Geophys. Res. Lett. 32, L17706. http://dx.doi.org/10.1029/2005GL023272.
Ensor, L.A., Robeson, S.M., 2008. Statistical characteristics of daily precipitation: comparisons of gridded and point datasets. J. Appl. Meteorol. Climatol. 47, 2468–2476.
Ford, T.W., Quiring, S.M., 2014. In-situ soil moisture coupled with extreme temperatures: a study based on the Oklahoma Mesonet. Geophys. Res. Lett. 41, 4727–4734. http://dx.doi.org/10.1002/2014GL060949.
Frich, P., Alexander, L.V., Della-Marta, P., Gleason, B., Haylock, M., Klein Tank, A.M.G., Peterson, T., 2002. Observed coherent changes in climatic extremes during the second half of the twentieth century. Clim. Res. 19, 193–212.
Griffiths, M.L., Bradley, R.S., 2007. Variations of twientieth-century temperature and precipitation extreme indicators in the northeast United States. J. Clim. 20, 5401–5417.
Groisman, P.Y., Knight, R.W., 2007. Prolonged dry episodes over the conterminious United States: New tendencies emerging during the last 40 years. J. Clim. 21, 1850–1862.
Groisman, P.Y., Knight, R.W., Karl, T.R., 2012. Changes in intense precipitation over the Central United States. J. Hydrometeorol. 13, 47–66. http://dx.doi.org/10.1175/JHM-d-11-039.1.
Grotjahn, R., Black, R., Leung, R., Wehner, M.F., Barlow, M., Bosilovich, M., Gershunov, A., Gutowski Jr., W.J., Gyakum, J.R., Katz, R.W., Lee, Y.-Y., Lim, Y.-K., Prabhat, 2015. North American extreme temperature events and related large scale meteorological patterns: a review of statistical methods, dynamics, modeling and trends. Clim. Dyn. 45, 1–34. http://dx.doi.org/10.1007/s00382-015-2638-6.
Gudmundsson, L., Bremnes, J.B., Haugen, J.E., Engen-Skaugen, T., 2012. Technical note: downscaling RCM precipitation to the station scale using statistical transformations – a comparison of methods. Hydrol. Earth Syst. Sci. 16, 3383–3390. http://dx.doi.org/10.5194/hess-16-3383-2012.
Guilbert, J., Betts, A.K., Rizzo, D.M., Beckage, B., Bomblies, A., 2015. Characterization of increased persistence and intensity of precipitation in the northeastern United States. Geophys. Res. Lett. 42, 1888–1893 0.1002/2015GL063124.
Gutowski Jr., W.J., Arritt, R.W., Kawozoe, S., Flory, D.M., Takle, E.S., Biner, S., Caya, D., Jones, R.G., Laprise, R., Leung, L.R., Mearns, L.O., Moufouma-Okia, W., Nunes, A. M.B., Qian, Y., Roads, J.O., Sloan, L.C., Snyder, M.A., 2010. Regional extreme monthly precipitation simulated by NARCCAP RCMs. J. Hydrometeorol. 7, 1373–1379.
Halmstad, A., Najafi, M.R., Moradhkani, H., 2013. Analysis of precipitation extremes with the assessment of regional climate models over the Willamette River Basin, USA. Hydrol. Process. 27, 2579–2590. http://dx.doi.org/10.1002/hyp.9376.
Hartmann, D.L., Klein Tank, A.M.G., Rusticucci, M., Alexander, L.V., Brönnimann, S., Charabi, Y., Dentener, F.J., Dlugokencky, E.J., Easterling, D.R., Kaplan, A., Soden, B.J., Thorne, P.W., Wild, M., Zhai, P.M., 2013. Observations: atmosphere and surface. In: Stocker, T.F., Qin, D., Plattner, G.-K., Tignor, M., Allen, S.K., Boschung, J., Nauels, J., Xia, Y., Bex, V., Midgley, P.M. (Eds.), Climate Change 2013: The Physical Science Basis. Contribution of Working Group I to the Fifth Assessment Report of the Intergovernmental Panel on Climate Change. Cambridge University Press, Cambridge, United Kingdom and New York, NY, USA.
Hawkins, E., Sutton, R., 2009. The potential to narrow uncertainty in regional climate predictions. Bull. Am. Meteorol. Soc. 90, 1095–1107.
Huerta, G., Sansó, B., 2007. Time-varying models for extreme values. Environ. Ecol. Stat. 14, 285–299.
Ji, D., Wang, L., Feng, J., Wu, Q., Cheng, H., Zhang, Q., Yang, J., Dong, W., Dai, Y., Gong, D., Zhang, R.-H., Wang, X., Liu, J., Moore, J.C., Chen, D., Zhou, M., 2014. Description and basic evaluation of Beijing Normal University Earth System Model (BNU-ESM) version 1. Geosci. Model Dev. 7, 2039–2064. http://dx.doi.org/10.5194/gmd-7-2039-2014.
Kenyon, J., Hegerl, G.C., 2010. Influence of modes of climate variability on global precipitation extremes. J. Clim. 23, 6248–6262. http://dx.doi.org/10.1175/2010JCLI3617.1.
Kharin, V.V., Zwiers, F.W., 2005. Estimating extremes in transient climate change simulations. J. Clim. 18, 1156–1173. http://dx.doi.org/10.1175/JCLI3320.1.
Kharin, V., Zwiers, F., Zhang, X., Hegerl, G.C., 2007. Changes in temperature and precipitation extremes in the IPCC ensemble of global coupled model simulations. J. Clim. 20, 1419–1444.
Kunkel, K.E., Karl, T.R., Brooks, H., Kossin, J., Lawrimore, J.H., Arndt, D., Bosart, L., Changnon, D., Cutter, S.L., Doesken, N., Emanuel, K., Groisman, P.Y., Katz, R.W., Knutson, T., O'Brien, J.J., Paciorek, C.J., Peterson, T.C., Redmond, K., Robinson, D., Trapp, J., Vose, R., Weaver, S., Wehner, M., Wolter, K., Wuebbles, D., 2013a. Monitoring and understanding trends in extreme storms. Bull. Am. Meteorol. Soc. 94, 499–514. http://dx.doi.org/10.1175/BAMS-D-11-00262.1.
Kunkel, K.E., Stevens, L.E., Stevens, S.E., Sun, L., Janssen, E., Wuebbles, D., Dobson, J. G., 2013b. Regional Climate Trends and Scenarios for the U.S. National Climate Assessment: Part 9. Climate of the Contiguous United States. NOAA Technical Report NESDIS 142-9. National Oceanic and Atmospheric Administration, National Environmental Satellite, Data, and Information Service, Washington, D.C. (85 pp.).
Loikith, P.C., Waliser, D., Lee, H., Neelin, J.D., Lintner, B.R., McGinnis, S., Mearns, L.O., Kim, J., 2015. Evaluation of large-scale meteorological patterns associated with temperature extremes in the NARCCAP regional climate model simulations. Clim. Dyn., 1–18. http://dx.doi.org/10.1007/s00382-105-2537-x.
Madsen, T., Figdor, E., 2007. When it Rains, it Pours: Global Warming and the Rising Frequency of Extreme Precipitation in the United States. Report prepared by Environment America Research and Policy Center, Boston.
Mannig, B., Müller, M., Starke, E., Merkenschlager, C., Mao, W., Zhi, X., Podzun, R., Jacob, D., Paeth, H., 2013. Dynamical downscaling of climate change in Central Asia. Glob. Planet. Chang. 110, 26–39.
Maraun D., Bias correction, quantile mapping, and downscaling: Revisiting the inflation issue, J. Clim. 26, 2137–2143.
Maraun, D., Wetterhall, F., Ireson, A.M., Chandler, R.E., Kendon, E.J., Widmann, M., Brienen, S., Rust, H.W., Sauter, T., Themebl, M., Venema, V.K.C., Chun, K.P., Goodess, C.M., Jones, R.G., Onof, C., Vrac, M., Thiele-Eich, I., 2010. Precipitation downscaling under climate change: recent developments to bridge the gap between dynamical models and the end user. Rev. Geophys. 48, 1–34.
Mass, C., Skalenakis, A., Warner, M., 2010. Extreme precipitation over the West Coast of North America: is there a trend? J. Hydrometeorol. 12, 310–318.
Mearns, L.O., Gutowski, W.J., Jones, R., Leung, L.-Y., McGinnis, S., Nunes, B., Qian, Y., 2009. A regional climate change assessment program for North America. EOS 90, 311–312.
Meehl, G.A., Arblaster, J.M., Branstator, G., 2012. Mechanisms contributing to the warming hold and the consequent U.S. East-West differential of heat extremes.

J. Clim. 25, 6394–6408.
Climate change impacts in the United States: the third National Climate Assessment. In: Melillo, J.M., Richmond, T.C., Yohe, G.W. (Eds.), U.S. Global Change Research Program, p. 841 10.7930/J0Z31WJ2.
Min, S.-K., Zhang, X., Zwiers, F.W., Hegerl, G.C., 2011. Human contribution to more-intense precipitation. Nature 470, 378–382.
Mishra, V., Ganguly, A.R., Nijssen, B., Lettenmaier, D.P., 2015. Changes in observed climate extremes in global urban areas. Environ. Res. Lett. 10. http://dx.doi.org/10.1088/1748-9326/10/2/024005.
Moss, R.H., Edmonds, J.A., Hibbard, K.A., Manning, M.R., Rose, S.K., van Vuuren, D.P., Carter, T.R., Emori, S., Kainuma, M., Kram, T., Meehl, G.A., Mitchell, J.F.B., Nakicenovic, N., Riahi, K., Smith, S.J., Stouffer, R.J., Thomson, A.M., Weyant, J.P., Wilbanks, T.J., 2010. The next generation of scenarios for climate change research and assessment. Nature 463, 747–756.
Ning, L., Riddle, E.E., Bradley, R.S., 2015. Projected changes in climate extremes over the northeastern United States. J. Clim. 28, 3289–3310. http://dx.doi.org/10.1175/JCLI-D-14-00150.1.
O'Gorman, P.A., Schneider, T., 2009. The physical basis for increases in precipitation extremes in simulations of 21st-century climate change. Proc. Natl. Acad. Sci. 106, 14773–14777. http://dx.doi.org/10.1073/pnas.0907610106.
O'Neill, M.S., Ebi, K.L., 2009. Temperature extremes and health: impacts of climate variability and change in 414 the United States. J. Occup. Environ. Medicine 51, 13–25. http://dx.doi.org/10.1097/JOM.0b013e318173e122.
Panofsky, H.A., Brier, G.W., 1968. Some Applications of Statistics to Meteorology. Penn State University, University Park, PA, p. 224.
Patz, J.A., Campbell-Lendrum, D., Holloway, T., Foley, J.A., 2005. Impact of regional climate change on human health. Nature 438, 310–317.
Peterson, T.C., Heim Jr., R.R., Hirsch, R., Kaiser, D.P., Brooks, H., Diffenbaugh, N.S., Dole, R.M., Giovannettone, J.P., Guirguis, K., Karl, T.R., Katz, R.W., Kunkel, K., Lettenmaier, D., McCabe, G.J., Paciorek, C.J., Ryberg, K.R., Schubert, S., Silva, V.B.S., Stewart, B.C., Vecchia, A.V., Villarini, G., Vose, R.S., Walsh, J., Wehner, M., Wolock, D., Wolter, K., Woodhouse, C.A., Wuebbles, D., 2013. Monitoring and understanding changes in heat waves, cold waves, floods and droughts in the United States: state of knowledge. Bull. Am. Meteorol. Soc. 94, 821–834.
Pidgeon, N., Fischoff, B., 2011. The role of social and decision sciences in communicating uncertain climate risks. Nat. Clim. Chang. 1, 35–41.
Pryor, S.C., Barthelmie, R.J., Schoof, J.T., 2013. High-resolution projections of climate-related risks for the Midwestern USA. Clim. Res. 56, 61–79.
Reyers, M., Pinto, J.G., Paeth, H., 2013. Statistical-dynamical downscaling of present day and future precipitation regimes in the Aksu river catchment in Central Asia. Glob. Planet. Chang. 107, 36–49.
Robeson, S.M., 2002. Relationships between mean and standard deviation of air temperature: implications for global warming. Clim. Res. 22, 205–213.
Robeson, S.M., Willmott, C.J., Jones, P.D., 2014. Trends in hemispheric warm and cold anomalies. Geophys. Res. Lett. 41, 9065–9071. http://dx.doi.org/10.1002/2014GL062323.
Rosenberg, E.A., Keys, P.W., Booth, D.B., Hartley, D., Burkey, J., Steinemann, A.C., Lettenmaier, D.P., 2010. Precipitation extremes and the impacts of climate change on stormwater infrastructure in Washington State. Clim. Chang. 102, 319–349. http://dx.doi.org/10.1007/s10584-010-9847-.
Rowan, E., Evans, C., Riley-Gilbert, M., Hyman, R., Kafalenos, R., Beucler, B., Rodehorst, B., Choate, A., Schultz, P., 2013. Assessing the sensitivity of transportation assets to extreme weather events and climate change. Transp. Res. Rec.: J. Transp. Res. Board 2326, 16–23. http://dx.doi.org/10.3141/2326-03.
Sanford, T., Frumhoff, P.C., Luers, A., Gulledge, J., 2014. The climate policy narrative for a dangerously warming world. Nature 4, 164–166.
Sato, N., Robeson, S.M., 2014. Trends in the near-zero range of the minimum air-temperature distribution. Phys. Geogr. 35, 429–442. http://dx.doi.org/10.1080/02723646.2014.927321.
Schaeffer, R., Szklo, A.S., Pereira de Lucena, A.F., Borba, B.S.M.C., Nogueira, L.P.P., Fleming, F.P., Troccoli, A., Harrison, M., Boulahya, M.S., 2012. Energy sector vulnerability to climate change: a review. Energy 38, 1–12.
Schoelzel, C., Friederichs, P., 2008. Multivariate non-normally distributed random variables in climate research – introduction to the copula approach. Nonlinear Process. Geophys. 15, 761–772.
Schoof, J.T., 2013. Statistical downscaling in climatology. Geogr. Compass 7, 249–265. http://dx.doi.org/10.1111/gec3.12036.
Schoof, J.T., 2015. High-resolution projections of 21st century daily precipitation for the contiguous U.S. J. Geophys. Res.: Atmos. 120, 3029–3042. http://dx.doi.org/10.1002/2014JD022376.
Sillmann, J., Kharin, V.V., Zhang, X., Zwiers, F.W., Bronaugh, D., 2013a. Climate extremes indices in the CMIP5 multimember ensemble: Part 1. Model evaluation in the present climate. J. Geophys. Res.: Atmos. 118, 1716–1733. http://dx.doi.org/10.1002/jgrd.50203.
Sillmann, J., Kharin, V.V., Zwiers, F.W., Zhang, X., Bronaugh, D., 2013b. Climate extremes indices in the CMIP5 multimember ensemble: Part 2. Future climate projections. J. Geophys. Res.: Atmos. 118, 2473–2493. http://dx.doi.org/10.1002/jgrd.50188.
Sivakumar, M.V.K., 2013. Weather and climate extremes: need for an importance of the journal. Weather Clim. Extrem. 1, 1–3.
Stevens, B., Giorgetta, M., Esch, M., Mauritsen, T., Crueger, T., Rast, S., Salzmann, M., Schmidt, H., Bader, J., Block, K., Brokopf, R., Fast, I., Kinne, S., Kornbleuh, L., Lohmann, U., Pincus, R., Reichler, T., Roeckner, E., 2013. The atmospheric component of the MPI-M Earth System Model: ECHAM6. J. Adv. Model. Earth Syst. 5, 146–172. http://dx.doi.org/10.1002/jame.20015.
Tang, Q., Zhang, X., Yang, X., Francis, J.A., 2013. Cold winter extremes in northern continents linked to Arctic sea ice loss. Environ. Res. Lett. 8, 014036. http://dx.doi.org/10.1088/1748-9326/8/1/014036.
Taylor, K.E., Stouffer, R.J., Meehl, G.A., 2012. An overview of CMIP5 and the experimental design. Bull. Am. Meteorol. Soc. 93, 485–498.
Teutschbein, C., Seibert, J., 2012. Bias correction of regional climate model simulations for hydrological climate-change impact studies: review and evaluation of different methods. J. Hydrol. 16, 12–29. http://dx.doi.org/10.1016/j.jhydrol.2012.05.052.
Thrasher, B., Maurer, E.P., McKellar, C., Duffy, P., 2012. Technical note: Bias correcting climate model simulated daily temperature extremes with quantile mapping. Hydrol. Earth Syst. Sci. 16, 3309–3314. http://dx.doi.org/10.5194/hess-16-3309-2012.
Trenberth, K.E., Dai, A., Rasmussen, R.M., Parsons, D.B., 2003. The changing character of precipitation. Bull. Am. Meteorol. Soc. 85, 1205–1217. http://dx.doi.org/10.1115/BAMS-85-9-1205.
Trenberth, K.E., Fasullo, J.T., Shepherd, T.G., 2015. Attribution of climate extreme events. Nat. Clim. Chang. 5, 725–730. http://dx.doi.org/10.1038/nclimate2657.
Tryhorn, L., DeGaetano, A., 2011. A comparison of techniques for downscaling extreme precipitation over the northeastern United States. Int. J. Climatol. 31, 1975–1989.
von Salzen, K., Scinocca, J.F., McFarlane, N.A., Li, J., Cole, J.N.S., Plummer, D., Verseghy, D., Reader, M.C., Ma, X., Lazare, M., Solheim, L., 2013. The Canadian Fourth Generation Atmospheric Global Climate Model (CanAM4). Part I: representation of physical processes. Atmos. Ocean 51, 104–125.
Wang, J., Zhang, X., 2008. Downscaling and projection of winter extreme daily precipitation over North America. J. Clim. 21, 923–937. http://dx.doi.org/10.1175/2007JCLI1671.1.
Wehner, M., 2013a. Methods of projecting future changes in extremes. In: Agha-Kouchak, A., et al. (Eds.), Extremes in a Changing Climate, Water Science and Technology Library 65; 2013ahttp://dx.doi.org/10.1007/978-94-007-4479-0 8.
Wehner, M., 2013b. Very intense seasonal precipitation in the NARCCAP ensemble: model performance and projections. Clim. Dyn. 40, 59–80.
Wilks, D.S., 1999. Multisite downscaling of daily precipitation with a stochastic weather generator. Clim. Res. 11, 125–136.
Willmott, C.J., Robeson, S.M., 1995. Climatologically aided interpolation (CAI) of terrestrial air temperature. Int. J. Climatol. 15, 221–229.
Wood, A.W., Leung, L.R., Sridhar, V., Lettenmaier, D.P., 2004. Hydrologic implications of dynamical and statistical approaches to downscaling climate model outputs. Clim. Chang. 62, 189–216.
Wuebbles, D., Meehl, G., Hayhoe, K., Karl, T.R., Kunkel, K., Santer, B., Wehner, M., Colle, B., Fischer, E.M., Fu, R., Goodman, A., Janssen, E., Kharin, V., Lee, H., Li, W., Long, L.N., Olsen, S.C., Pan, Z., Seth, A., Sheffield, J., Sun, L., 2013. CMIP5 climate model analyses: climate extremes in the United States. Bull. Am. Meteorol. Soc. 95, 571–583.
Xin, X., Wu, T., Zhang, J., 2012. Introductions to the CMIP 5 simulations conducted by the BCC climate system model (in Chinese). Adv. Clim. Chang. Res. 4, 41–49.
Yukimoto, S., Adachi, Y., Hosaka, M., Sakami, T., Yoshimura, H., Hirabara, M., Tanaka, T.Y., Shindo, E., Tsujino, H., Deushi, M., Mizuta, R., Yabu, S., Obata, A., Nakano, H., Koshiro, T., Ose, T., Kitoh, A., 2012. A new global climate model of the Meteorological Research Institute: MRI-CGCM3-Model description and basic performance. J. Meteorol. Soc. Jpn. 90A, 23–64.
Zhang, X., Alexander, L., Hegerl, G.C., Jones, P., Klein Tank, A., Peterson, T.C., Trewin, B., Zwiers, F.W., 2011. Indices for monitoring changes in extremes based on daily temperature and precipitation data. WIREs Clim. Chang. 2, 851–870. http://dx.doi.org/10.1002/wcc.147.
Zwiers, F.W., Zhang, X., Feng, Y., 2011. Anthropogenic influence on long return period daily temperature extremes at regional scales. J. Clim. 24, 881–892.